Parallel DSMC Simulation of a Single Under-Expanded Free Orifice Jet From Transition to Near-Continuum Regime

J.-S. Wu
Phone: 886-3-573-1693
Fax: 886-3-572-0634
e-mail: chongsin@faculty.nctu.edu.tw

S.-Y. Chou

U.-M. Lee

Y.-L. Shao

Y.-Y. Lian

Department of Mechanical Engineering, National Chiao-Tung University, Hsinchu 30050, Taiwan

This paper describes the numerical analysis of the flow structure of a single underexpanded argon free jet issuing into a lower-pressure or vacuum environment using the parallel three-dimensional direct simulation Monte Carlo (DSMC) method employing dynamic domain decomposition. Unstructured and tetrahedral solution-based refined mesh depending on the local mean free path is used to improve the resolution of solution. Simulated Knudsen numbers of the stagnation conditions based on orifice diameter, Reynolds numbers based on the conditions at the orifice exit, and stagnation-to-background pressure ratios are in the range of 0.0005–0.1, 7–1472, and 5–∞, respectively, where "∞" represents vacuum condition in the background environment. Results show that centerline density decays in a rate proportional to the inverse of the square of the axial distance (z^{-2}) from the orifice for all ranges of flow in the current study. The more rarefied the background condition is, the longer the z^{-2}-regime is. In addition, a distinct flow structure, including barrel shock, Mach disk and jet boundary, is clearly identified as the Knudsen number reaches as low as 0.001. Predicted location and size of Mach disk in the near-continuum limit (Kn = 0.001, 0.0005) are found to be in reasonable agreement with experimental results in the continuum regime. [DOI: 10.1115/1.2062807]

Introduction

Many industrial processes requires the use of high-speed underexpanded jets to either provide impulse or deliver the interested gas species to the designated region or provide high-density cooling to specific heated wall (due to small area of jet impingement and higher velocities of impact). Practical examples include the use of jets for rocket exhausts at high altitude and attitude control on satellite, cooling of Micro-Electro-Mechanical-Systems (MEMS) devices, fine particle deposition and removal, in inkjet printing technology, showerhead (periodic array of microjets) for materials processing, among others [[1], and the reference cited therein]. The nozzle used to generate the under-expanded jet can be either a simple thin sonic orifice or converging-diverging (Laval) nozzle [2]. The latter design can create uniform supersonic jets with desirable flow properties. For example, one such property is a highly uniform pressure along the centerline of the jet that extends many nozzle diameters downstream (inviscid potential core). Of course, this design may also present some significant drawbacks, including difficulties of manufacturing and high noise level. Previous studies have shown that these drawbacks may be removed if the nozzle is miniaturized [2]. However, manufacturing this kind of nozzle is not straightforward at all.

On the other hand, *thin sonic orifice*, having a minimum cross-sectional area at the exit, represents the simplest type of micronozzle. One of the obvious advantages of using the orifice lies upon the simplicity of manufacturing and maintenance. This type of orifice generates an *underexpanded sonic jet* if the pressure ratio of chamber to background is approximately larger than 2, which is often the case in practical applications. However, the axial pressure distribution resulting from the orifice microjet varies significantly within the first few orifice diameters. The inviscid potential core of the supersonic jet dissipates and the resulting subsonic flow decays rapidly, which may be advantageous for mixing purpose. The situation is even more complicated due to rarefaction if the background environment is at low-pressure or near-vacuum. Thus, understanding of the flow characteristics of the free orifice underexpanded sonic jets is important when applying them to these practical situations.

A single underexpanded orifice jet issuing into a quiescent environment has been studied extensively in the past, but most studies were either emphasizing upon the experimental visualization of the flow structure [[3,9], and references cited therein] or simple analytical solution [4,5]. Very few simulation studies were done, especially when rarefaction effects are considered [12]. The main features of the continuum free jet in the near field include a Mach disk, barrel shock and free jet boundary [1]. Behind the Mach disk, subsonic core and supersonic outer flow are bounded by a slip line, which emanates from the triple point. The triple point is the intersection location of barrel shock and Mach disk. The barrel shock intersects with the Mach disk and then reflects as an oblique shock.

Several theoretical researches [4,5] studied the flow structures, especially the diameter or location of the Mach disk. However, there is no satisfied analytical method available to predict the entire structure of an underexpanded sonic jet. Numerical solutions using method of characteristics [6,7] predicted the inviscid jet boundary and the intercepting shock, but were generally not able to predict the formation of Mach disk. Instead, experiments using flow visualization were able to capture the location and diameter of the Mach disk. Ashkenas and Sherman [8] measured the Mach disk position using electron beam visualization in the continuum limit. They proposed a well-known correlation as $x_M/D = 0.67(p_0/p_b)^{1/2}$, where x_M is the Mach disk position, p_0 is the source pressure, and p_b is the background pressure. Later, in the same group of Sherman [9], they measured the Mach disk position and diameter of a highly underexpanded sonic jet, considering high-pressure ratios, high stagnation pressures, temperature variations and geometries of solid boundary in the nozzle lip

Contributed by the Fluids Engineering Division for publication in the JOURNAL OF FLUIDS ENGINEERING. Manuscript received by the Fluids Engineering Division March 5, 2004; final manuscript received: June 26, 2005. Associate Editor: Fernando Grinstein.

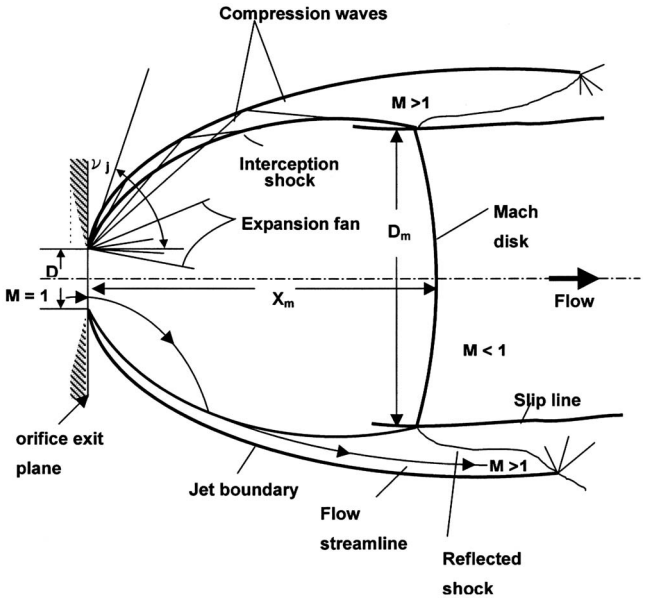

Fig. 1 Flow structure of a single under-expanded orifice jet in the continuum regimen [1]

region. Results showed that Mach disk location was insensitive to the variations of (a) γ, (b) condensation, (c) nozzle lip geometry, (d) absolute pressure level.

Muntz et al. [10] proposed a rarefaction parameter $D(p_o p_b)^{1/2}/T_0$ to classify the structure of a free jet expanding into a region of finite background pressure. This rarefaction parameter is in fact proportional to the inverse of $(p_o/p_b)^{1/2}$ Kn, which combines the effects of pressure ratio and rarefaction. The structures of free jet can be classified into three flow regimes: continuum, transition, and scattering, according to the degree of continuum to rarefied upstream. In this scattering flow regime, any evidence of continuum gas dynamic features disappears [2]. In this regime, the shock envelope has completely vanishes and the gas density smoothly passes to the background density through scattering process. Only the DSMC method [11] is capable of simulating such flow field, although it is well known that it is very computational expensive. Usami and Teshima [12] did an experiment using mass-sampling technique for mass flow measurements in an underexpanded orifice jet. Flow field was then simulated by the DSMC method and reasonable agreement was found as compared with experiments, although the treatment of outflow boundary conditions is problematic due to the assumption of mean zero velocities in the DSMC simulation and near-uniform mesh. It is rather difficult to simulate this type of flow field since the density varies very much from the orifice to the outer boundaries, which makes the selection of both the time-step size and cell size very challenging in the DSMC simulation.

In summary, numerical studies along this line are relatively few or unsatisfied, especially the rarefaction effects caused by the low-pressure stagnation condition and low-pressure background, in which the N-S equations break down. In addition, the flow may reach hypersonic speed ahead of the Mach disk (or highly thermal nonequilibrium) for larger pressure ratio, which makes the simulation using N-S equation difficult. Thus, in the current study we shall use the DSMC method to systematically study the flow structure of the underexpanded sonic jets at different flow conditions with Knudsen numbers in the range of 0.0005–0.1 and Reynolds numbers in the range of 7–1472, both defined using orifice size and upstream stagnation conditions of pressure and temperature (Fig. 1). Transition to turbulence is not considered in the current simulation due to the low Reynolds-number flows. Simulated results are then compared with experimental data available in the literature.

The paper begins with descriptions of numerical method and procedures (Table 1). Then, results are presented along with appropriate discussions. Finally, conclusions of this study are presented.

Numerical Method and Procedures

In the current study, the single under-expanded free jet flow is intrinsically axisymmetric. However, the three-dimensional DSMC code was used instead of the axisymmetric DSMC code because of the following two reasons. First, it is well known that the accuracy near the axis deteriorates if the cell size becomes small (thus, small cell volume) due to insufficient samplings,

Table 1 Corresponding values of the rarefaction parameter for test conditions

Po / Pb	Kn			
	0.0005	**0.001**	**0.01**	**0.1**
5	**15.98**	**7.991**	**0.799**	**0.0790**
10	**11.30**	**5.651**	**0.565**	**0.0560**
20	**7.992**	**3.995**	**0.399**	**0.0390**
50	**5.050**	**2.527**	**0.253**	**0.0253**
100	**3.570**	**1.787**	**0.179**	**0.0179**
150	**2.920**	**1.459**	**0.146**	**0.0146**
200	**2.530**	**1.264**	**0.126**	**0.0126**
250	**2.260**	**1.130**	**0.113**	**0.0113**
500	**1.600**	**0.799**	**0.080**	**0.0080**
1000	**1.130**	**0.565**	**0.057**	**0.0057**
2500	**0.710**	**0.357**	**0.036**	**0.0036**
5000	**0.510**	**0.253**	**0.025**	**0.0025**
7500	**0.410**	**0.206**	**0.020**	**0.0020**
10000	**0.360**	**0.179**	**0.018**	**0.0018**
∞	0.000	0.000	0.000	0.0000

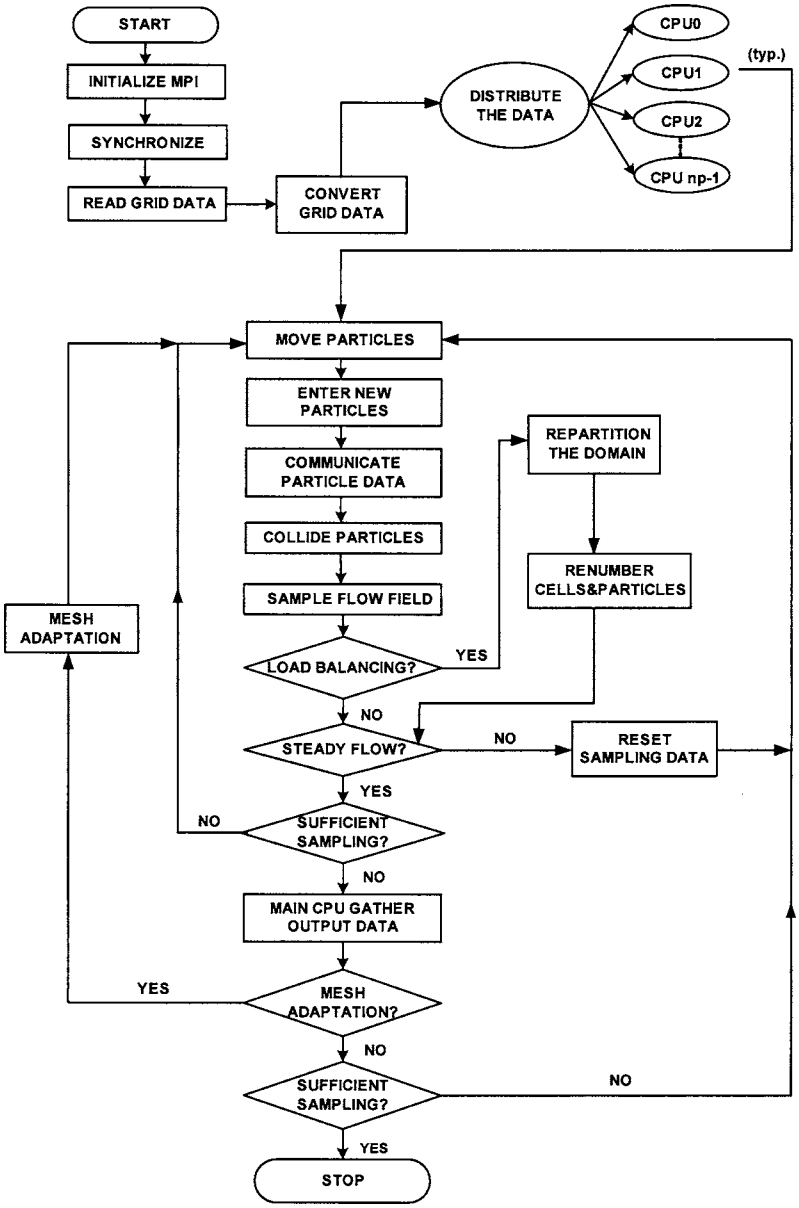

Fig. 2 Flow chart of the parallel DSMC method (PDSC) with mesh refinement

which often contradicts with the requirements of spatial resolution. In addition, position-based (e.g., radial) particle (or cell) weighting [11] used to remove this inaccuracy often induce other problems, such as random walk, whose effect is hard to evaluate before simulation. However, use of the three-dimensional DSMC code will naturally remove this constraint, although the computational load is higher than the axisymmetric DSMC code in essence. Nevertheless, it can be relieved to greater extent by taking the advantage of the symmetric conditions and efficient parallel processing, which will be shown clearly later. Second, maintaining both the axisymmetric and three-dimensional DSMC codes can be very time-consuming and tedious. Especially, we are interested in applying this 3D code to compute multiple jet interaction in the near future. The DSMC method and the parallel DSMC code (PDSC) [13] used in the current study are described as follows in turn.

The DSMC Method. The direct simulation Monte Carlo method (DSMC) [11] is a particle method for the simulation of gas flows. The gas is modeled at the microscopic level using simulated particles which each represents a large number of physical molecules or atoms. The physics of the gas are modeled through the motion of particles and collisions between them. Mass, momentum and energy transports are considered at the particle level. The method is statistical in essence. Physical events such as collisions are handled probabilistically using largely phenomenological models, which are designed to reproduce real fluid behavior when examined at the macroscopic level. General procedures of the DSMC method consist of four major steps: moving, indexing, collision and sampling. In the current study, we use VHS molecular model [11] to reproduce real fluid behavior as well as no time counter (NTC) [11] for the collision mechanics. Since monatomic gas (argon) is simulated, no energy-exchange model is required. Details of the procedures and the consequences of the computational approximations regarding DSMC can be found in Bird [11].

The Parallel DSMC Method. In the present study, we have utilized the previous developed ***P***arallel three-dimensional ***DS***MC ***C***ode (PDSC) [13], which features unstructured adaptive mesh

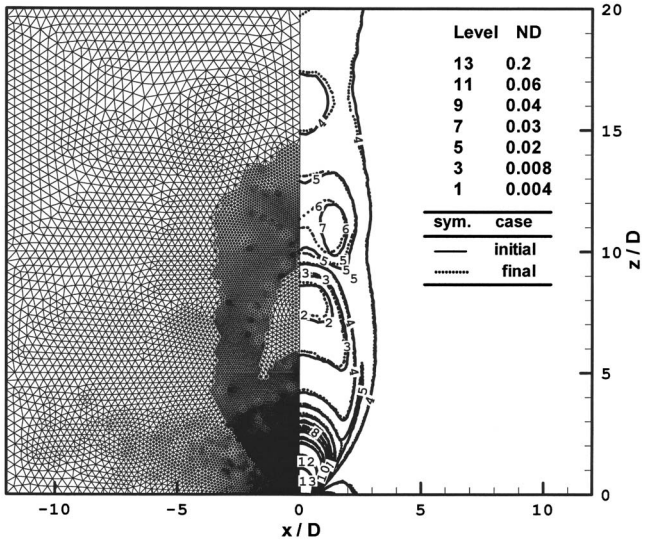

Fig. 3 Surface mesh and its isodensity distribution on a 1/16-domain of a single jet (Kn=0.001, PR=150) (initial: 149, 168 cells; level-2: 1,109,411 cells)

refinement [14,17], parallel implementation on memory-distributed machines using dynamical domain decomposition [15,16], variable time-step method [13,17], and boundary-pressure iterative scheme [19]. Details of all features of the PDSC can be found in these references and will be only briefly described here for completeness, considering the specific application in the current study.

Overall computational procedures of the PDSC can be summarized schematically in Fig. 2. The parallel DSMC method is implemented on an unstructured tetrahedral mesh using the particle ray-tracing technique [17,18], which takes the advantage of the cell connectivity information. Variable time-step approach is used by enforcing mass, momentum and energy conservations when simulation particles cross the interface between cells [13,17]. Mean velocities and temperatures at the outflow boundaries can be obtained by iteratively enforcing the specified pressure boundary conditions [19]. During the simulation, the mesh *h-refinement* technique (adding local grid points) with cell-quality control is used to repeatedly improve the cell distribution according to the solution, based on some adaptation criteria (for example, "density" in the current study) [13,14]. Multilevel graph-partitioning technique [20] is used to dynamically redecompose the computational domain to balance the workload among processors [15,16]. Stop at Rise (SAR) [21] scheme is used to determine when to repartition the computational domain by defining a degradation function, which represents the average idle time per time step for each processor including the cost of repartition. Communication of particle data between processors only occurs when particle hits the inter-processor boundary, while communication of cell data only occurs when repartitioning the domain takes effect. Data for communication is sent and received as a whole to reduce the communicational time between processors.

Table 3 List of computing domains for Kn=0.0005 and 0.001

PR	x/D	z/D
5	3	5
10,20	3	10
50-200	6	20
250-∞	20	60

The current parallel code, in the Single Program Multiple Data (SPMD) paradigm, is implemented on the parallel memory-distributed system, e.g., PC-cluster system (one master processor and 23 slave processors with each having 2.4 GHz AMD, 0.5 G RAM, and Giga-bit ethernet in our laboratory). This code is highly portable since the standard message-passing interface (MPI) is used to communicate information among processors. Results presented in the following are obtained using 23 processors unless otherwise specified.

Results and Discussions

Before the detailed discussion of computational results the single orifice jet interested in the current study, we would like to mention that the parallel DSMC code [13] that we are using has been verified for a parallel twin-jet interaction at similar Knudsen number (Kn=0.00385) by comparing well with the experimental data in Ref. [13]. This nevertheless justifies our usage of the parallel DSMC code [13].

Flow Conditions and Simulation Conditions. A single jet, issuing into a chamber region at specified background pressure, is simulated in the current study. Monatomic argon gas is used as the

Table 2 Simulation conditions for Kn=0.0005

Kn=0.0005							
PR	total computing cells	total particles	averaged particles per cell	total iterations	transition iterations	sampling iterations	reference time scale
5	1,147,279	12,575,099	11	40,000	6,000	34,000	1E-10
10	1,182,070	13,512,907	11	40,000	6,000	34,000	1E-10
20	1,136,273	12,647,114	11	40,000	6,000	34,000	1E-10
50	1,254,763	18,512,998	15	40,000	6,000	34,000	1E-11
250	990,371	19,007,100	19	40,000	6,000	34,000	1E-9
500	950,590	9,871,825	10	40,000	6,000	34,000	1E-9
1000	99,7421	9,458,497	9	40,000	6,000	34,000	1E-9
2500	988,688	8,058,022	8	40,000	6,000	34,000	1E-9
5000	964,351	6,698,308	7	40,000	6,000	34,000	1E-9
∞	968,080	8,498,017	9	40,000	6,000	34,000	1E-9

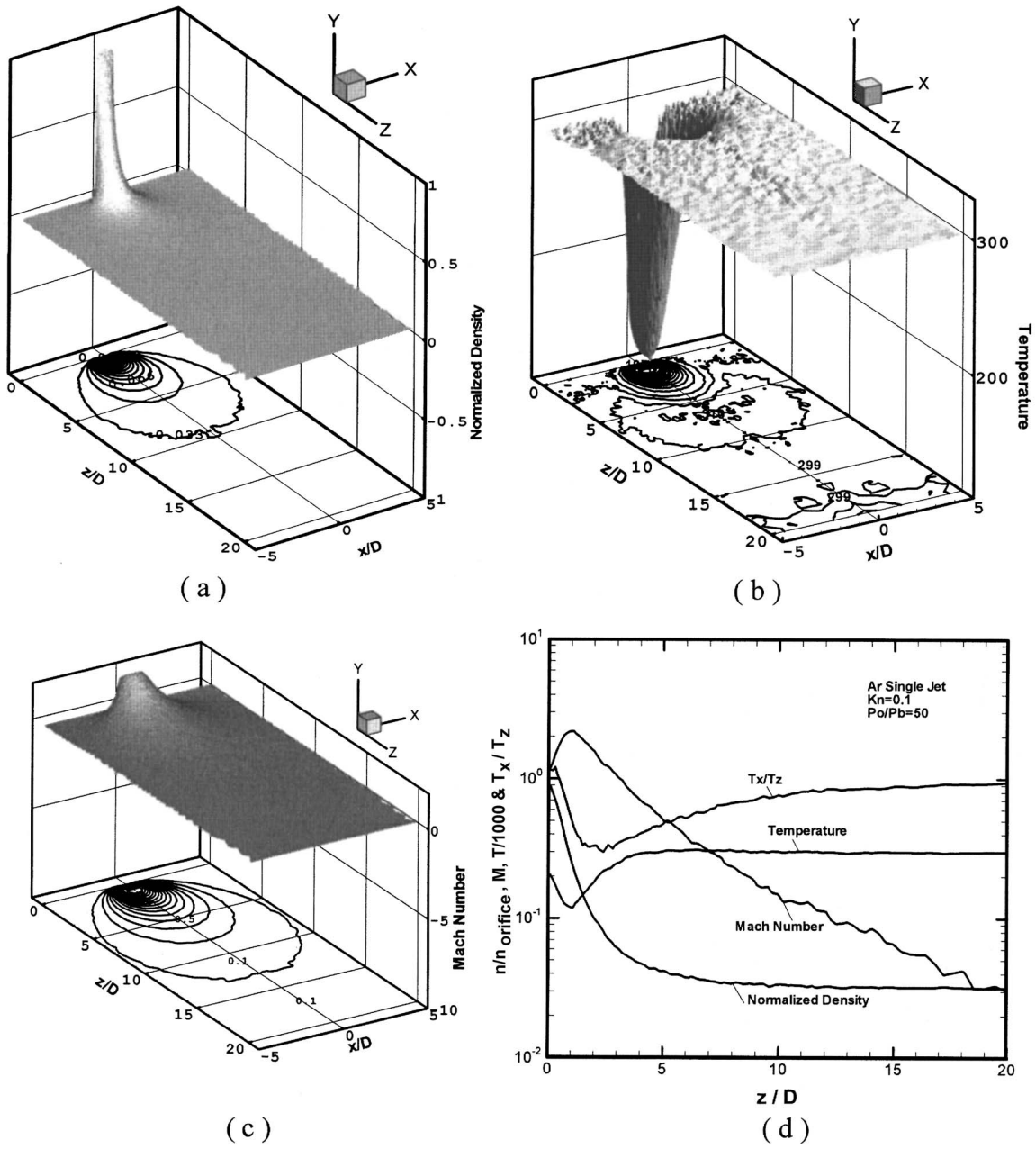

Fig. 4 Properties distribution at Kn=0.1, PR=50 of underexpanded argon jet (y=0 plane) (a) normalized density; (b) temperature; (c) Mach number; (d) data along centerline

working gas to preclude any complexities caused by the energy exchange among internal degrees of freedom. Orifice size used for generating the under-expanded free jet is 500 μm in diameter. Uniform sonic flow condition at the exit of the thin orifice is assumed, although viscous effects may be present in this low Reynolds-number flow regime that we are interested in. However, it is well known that for highly underexpanded free jets, the high supersonic region only weakly depends on the transonic conditions at the orifice [8]. Thus, inviscid gas dynamics (quasi-1D) is used to define the exit conditions at the orifice using the assumption. Parametric studies, varying Knudsen numbers ($\mathrm{Kn}=\lambda_{\mathrm{upstream}}/d_{\mathrm{orifice}}$) in the range of 0.0005–0.1 and stagnation-to-background pressure ratios ($\mathrm{PR}=p_0/p_b$) in the range of $5-\infty$, are considered. Corresponding upstream (stagnation) pressures and temperature are in the range of 107–21,446 Pa and 300 K, respectively. Pressure and temperature at outflow boundaries are fixed as specified background pressure and 300 K, respectively. Resulting Reynolds number defined using the conditions at the orifice exit is in the range of 7–1472, which is very low as compared with previous studies [8] that considered the macro jets in the continuum regime (upstream). Thus, the possibility of transition from laminar to turbulence is not considered in the current simulation.

We first run some typical cases (at same Knudsen number) to observe if the steady state is reached by observing if the total number of particles is approximately constant. We then decide the number of time steps (iterations) required to reach steady state conservatively by putting some safety factor, e.g., 2–3 times the number of iterations to reach approximate constant particle numbers. For convenience, we often use the same number of iterations (time steps) for representing the transient periods at different pressure ratios for the same Knudsen number. We believe this should be safe for all the cases considered that steady state has been reached for sampling.

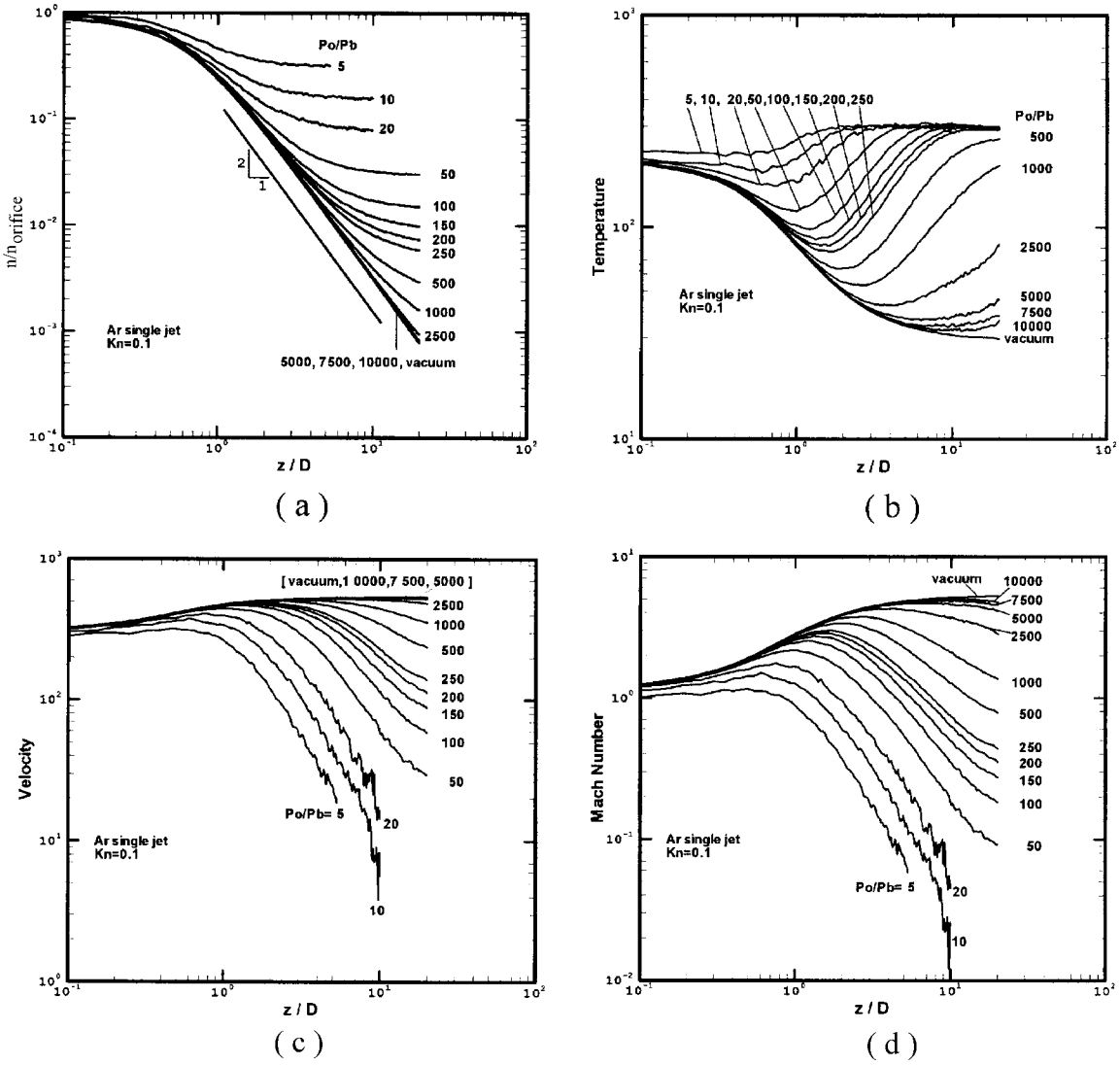

Fig. 5 Centerline normalized density, temperature, velocity, and Mach number distributions at different pressure ratios (Kn=0.1)

Typical refined unstructured mesh at the final level (level-2) along with the distribution of isodensity is shown in Fig. 3 (Kn =0.001, PR=150). It clearly shows that the mesh is automatically refined near the high-density regions. In this specific case, the number of cells increases from 149,168 cells initially to 1,109,411 cells at level-2 mesh refinement. Total number of particles in this case is approximately 10 millions. Resulting number of particles per cell is on the order of 10, except in the region near the orifice exit (~2). In general, the number of simulated particles is in the range of 0.1 million (Kn=0.1, PR=∞) to 19 million (Kn =0.0005, PR=250), while the number of time steps (iterations) for sampling is about 34,000 for each case. Detailed simulation conditions for the most challenging case (Kn=0.0005) are listed in Table 2. The number of particles used in this Kn=0.0005 case is on the order of 10 million. The reference time step (1E-10) represents the smallest time step used in the computational domain due to the high-density region, thus, very small cell, near the exit of the orifice. The mean velocities at the outer boundaries are obtained during the simulation by iteratively enforcing the specified pressure that uses the concept of flux conservation through the boundaries, which is similar to that in [19]. Temperatures at the outflow boundaries are set as 300 K. Since the flow is axisymmetric, only 1/16 of the physical domain is considered, where the specular boundary condition is imposed on each of the sliced plane. Results using this sliced domain are found to be in excellent agreement with those using full domain. In general, the larger the pressure ratio is, the larger the computational domain is required. Detailed sizes of computational domain for Kn=0.0005 and Kn=0.001 at different pressure ratios are listed in Table 3 for reference. In the following, we will discuss the effects of pressure ratio and rarefaction on the general flow structures, when presenting the simulation results.

Effects of Pressure Ratio

Kn=0.1. Before looking into the effects of pressure ratio, we first present the typical distributions of the normalized density, temperature and Mach number at the sliced plane ($y=0$) that are illustrated in Figs. 4(*a*)–4(*c*), respectively, for Kn=0.1 and PR =50. Centerline distribution of the above parameters (up to z/D =20) along with the ratio of thermal nonequilibrium (T_x/T_z) is also shown together in Fig. 4(*d*) for the convenience of comparison. Results at this flow condition show that the density monotonically decreases very rapidly outward in all directions from the orifice exit due to the lower pressure in the background (~0.03 of the value at the orifice exit). Temperature decreases due to rapid expansion near the orifice region, reaching as low as 12 K at

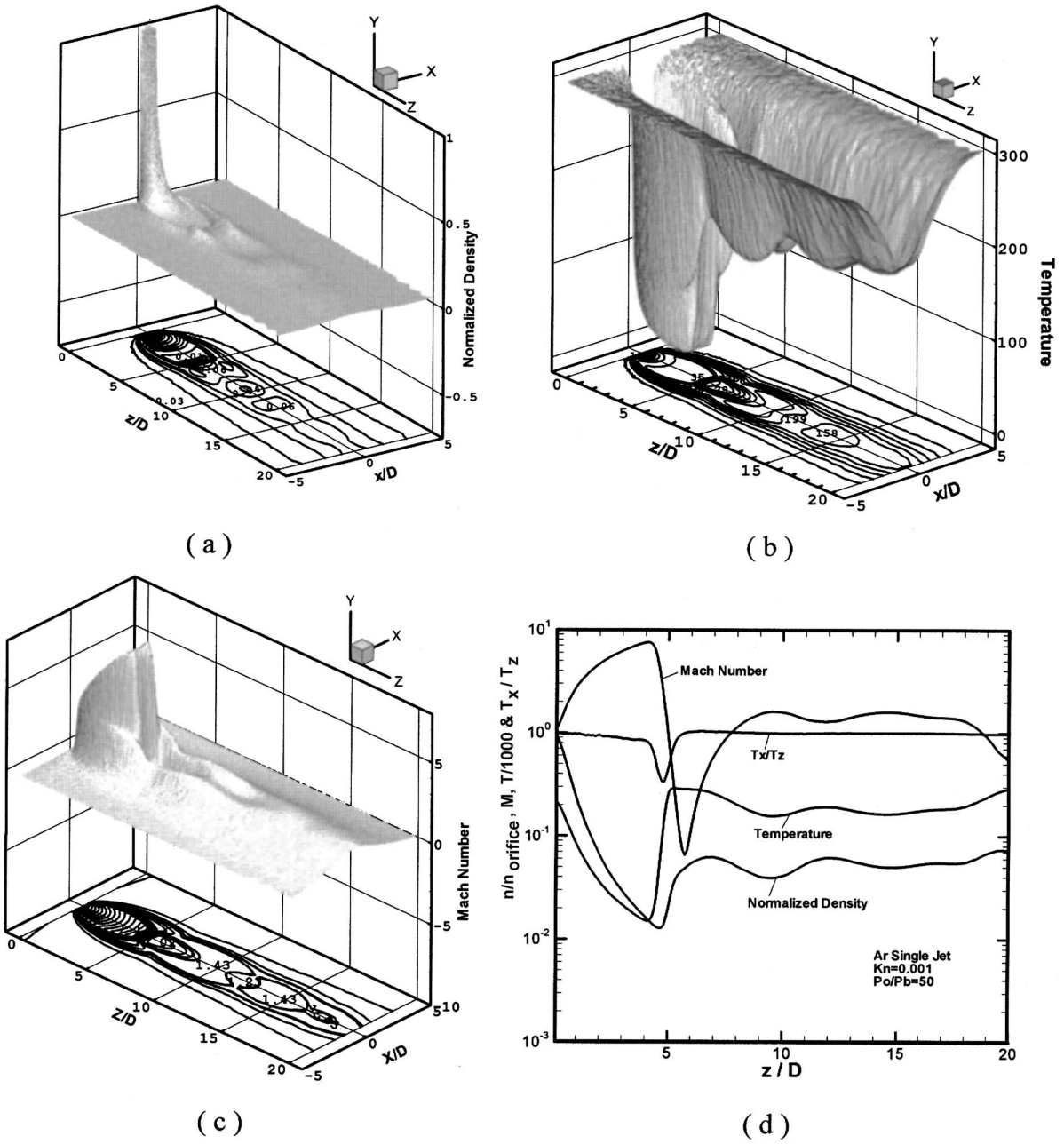

Fig. 6 Properties distribution at Kn=0.001, PR=50 of argon jet (*y*=0 plane) (a) normalized density; (b) temperature; (c) Mach number; (d) data along centerline

$z/D \approx 1$, and then increase to the specified background temperature, 300 K, at $z/D \approx 5$. Mach number increases up to 2.2 at about the same location ($z/D \approx 1$) and then decrease down to 0.1 at $z/D \approx 20$. The ratio of thermal nonequilibrium deviates from unity in the near orifice region with a value of 0.3 at $z/D=2.5$, which shows a strong thermal nonequilibrium exists in this flow due to rapid expansion.

Figures 5(*a*)–5(*d*) show the effects of pressure ratio to the centerline distributions of normalized density, temperature, velocity, and Mach number, respectively, at Kn=0.1, which is in the transitional regime. Pressure ratio in the current study is in the range of $5-\infty$, which ensures the choke condition at the orifice exit. In general, density [Fig. 5(*a*)] decreases monotonically along the centerline to the background value as expected. For example, the density at $x/D=20$ decreases down to 0.1% of the value at the orifice exit for PR $\geqslant$ 5,000. In addition, normalized density data along the centerline can be fitted as $n/n_{\text{orifice}}=0.24(z/D)^{-2}$ for PR $\geqslant$ 5,000 in the current simulation range ($z/D \leqslant 20$), which is nearly the same as that obtained experimentally [8]. Note that the axial distance, where the −2-slope decay holds, begins at $x/D \approx 1$. In Fig. 5(*b*), temperature generally decreases first along the centerline due to expansion and then increases to the background temperature. Minimum temperature is in the range of 30–220 K for PR in the range of $\infty-5$. Generally, the axial distance, where the minimum temperature reaches, increases with increasing pressure ratio. In Fig. 5(*c*), centerline velocity generally increases at first and then decreases further downstream. Faster decrease in the downstream is found for lower pressure ratios, which is retarded by the existence of higher-density background gas. For higher-pressure ratios, the centerline velocity stays at nearly constant value all the way downstream (PR $\geqslant$ 5,000). In Fig. 5(*d*), Mach

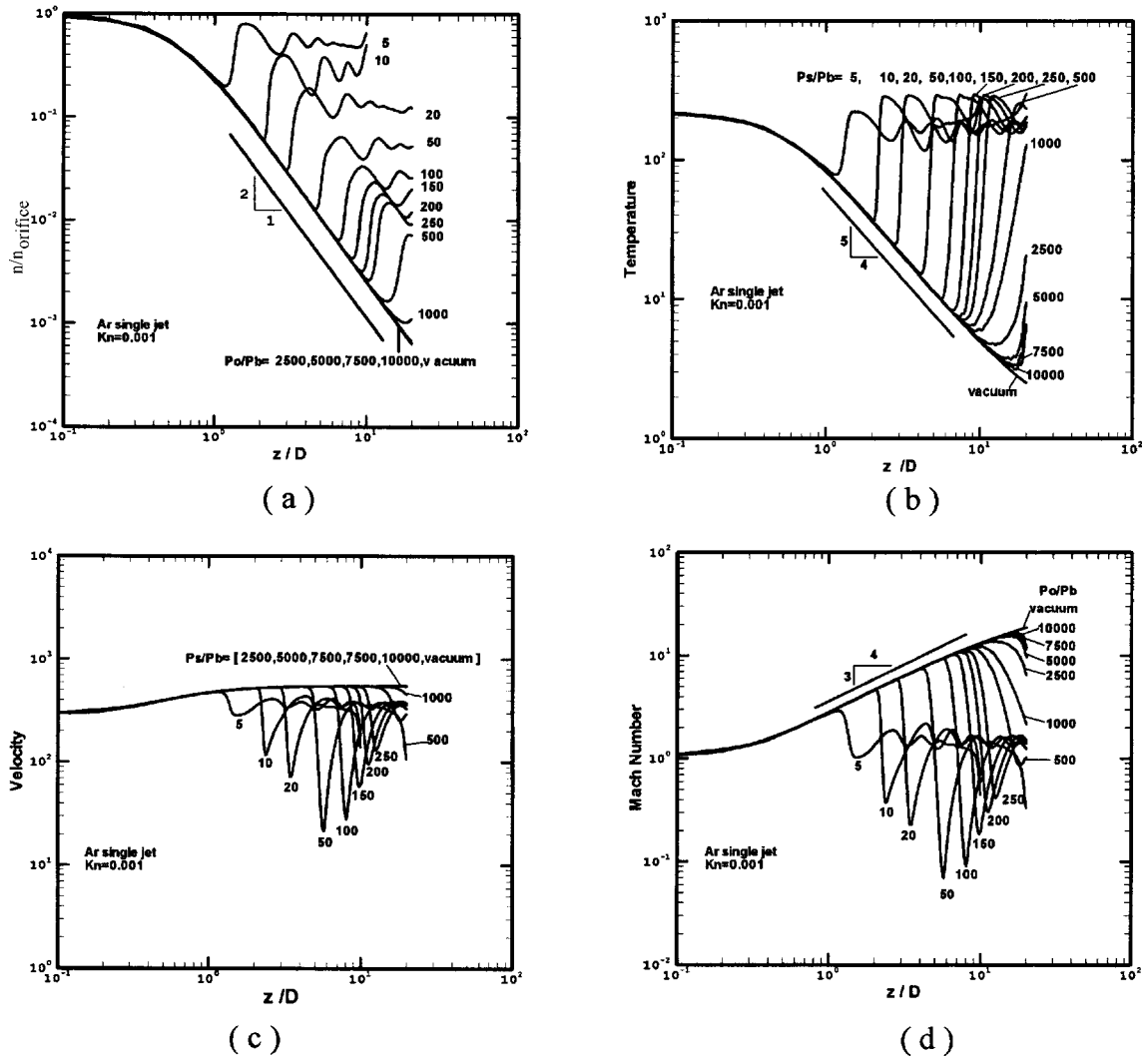

Fig. 7 Centerline normalized density, temperature, velocity and Mach number distributions at different pressure ratios (Kn=0.001)

number along the centerline generally increases to supersonic speed at first due to expansion and then decreases to low subsonic speed at far downstream for lower pressure ratios. It can be found that the change of Mach number with respect to the downstream location is generally larger than the centerline velocity because the speed of sound also varies depending on translational temperature. Note that maximum Mach number is in the range of 1.2–5 for PR in the range of 5–∞. Axial distance, where the maximum Mach number reaches, also increases with pressure ratio. In general, the above results show that at this Kn=0.1 the larger the pressure ratio, the more the gas expansion from the orifice into the background.

Kn=0.001. Typical property distributions (normalized density, temperature and Mach number) at the sliced plane ($y=0$) along with the centerline property distributions in the near-continuum regime (Kn=0.001) are illustrated in Figs. 6(*a*)–6(*d*), respectively. Unlike the case in the transitional regime (Fig. 4), a distinct cell-like flow structure, including shock and expansion waves, begins to appear. Results show that the density decreases very rapidly in the streamwise direction from the orifice exit and is approximately 1%, of the value at the orifice exit, at $z/D \approx 5$. It then increases up to 6%, of the value at the orifice exit, at $z/D \approx 7$ due to the formation of a thickened Mach disk. After this, the density decreases and increases again repeatedly, although the amplitude of alternation becomes smaller. In addition, a barrel shock circulating the core region that prevents the penetration of background gas into the core region. Due to rapid gas expansion, temperature decreases down to 15 K at location before the thickened Mach disk, and then increases to 300 K after the thickened Mach disk. It then follows the similar trend as the density variations afterwords. As for Mach number, it increases up to hypersonic speed (7.3) before the thickened Mach disk ($z/D \approx 4.5$), and drops to very low subsonic speed (0.07) right after the thickened Mach disk ($z/D \approx 5.5$). In Fig. 6(*d*), it also shows the ratio of thermal nonequilibrium (T_x/T_z) along the centerline. Results show that strong thermal nonequilibrium exists near the Mach disk location with a value of 0.3 due to strong compression of gas molecules across the shock, whose data can only be simulated using particle method as in the current study. In addition, strong thermal nonequilibrium also appears near the lips of the orifice due to rapid gas expansion, although it is not shown in the current report. In general, the cell-like flow structure begins to appear explicitly with several thickened shock structure at this near-continuum regime (Kn=0.001). The structure will be more observable as rarefaction is reduced. Comparison of the simulated Mach-disk position and diameter with experimental data in the near-continuum regime will be discussed later.

Figures 7(*a*)–7(*d*) illustrate the effects of pressure ratio (PR

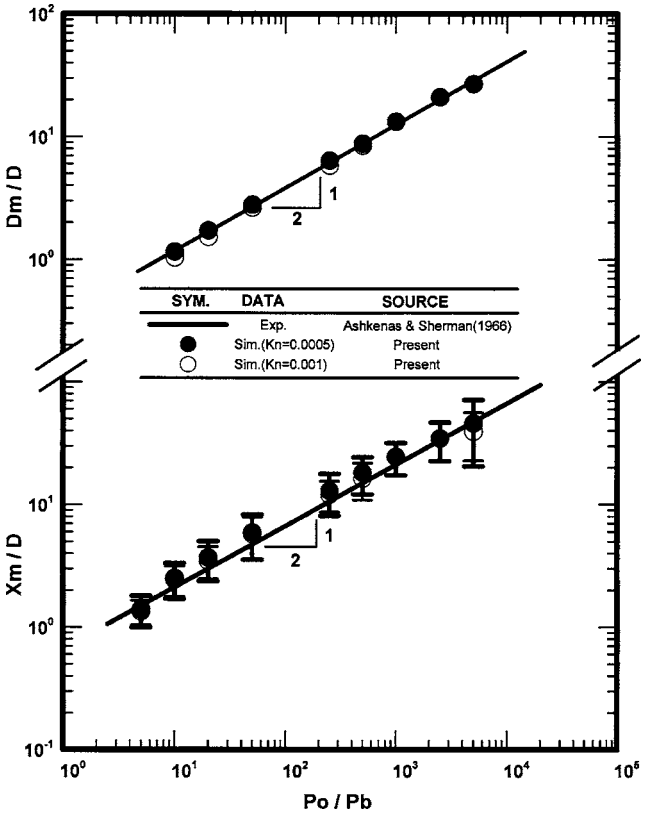

Fig. 8 Position and diameter of Mach disk as a function of pressure ratio for a single argon underexpanded jet

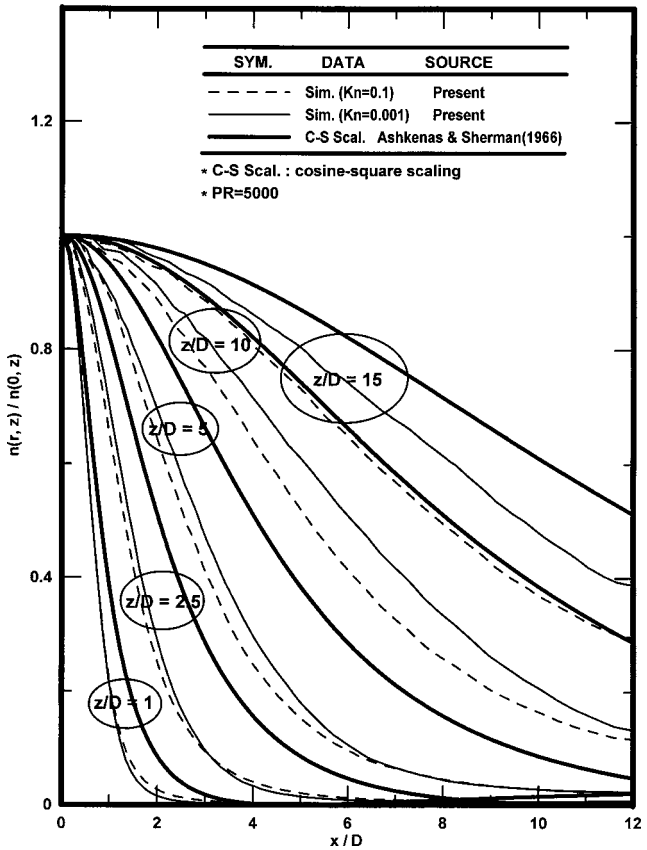

Fig. 9 Comparison of the radial profiles of normalized density at different positions at (PR=5000)

=5–∞) to the centerline distributions of normalized density, temperature, velocity and Mach number, respectively, at Kn=0.001, which is in the near-continuum regime. Again the density decreases rapidly along the centerline before the appearance of the Mach disk and scales as $n/n_{\text{orifice}}=0.24(z/D)^{-2}$ starting at $z/d \approx 1$, which is nearly the same as the case in Kn=0.1. However, Mach disk either disappears or becomes unrecognizable when PR $\geqslant$ 2500 probably due to the very rarefied flow (low background pressure) at the very downstream. We have extended the region of simulation up to $z/D=120$ for larger pressure ratios and have found the Mach disk is not clear at all. This more or less can be explained or correlated by using a rarefaction parameter, which will be shown shortly. Increase of the density across the Mach disk is generally the same in the range of 6–7 times for pressure ratios in the range of 10–500 [Fig. 7(*a*)], except the case of PR =5, in which it increases only approximately 2.5 times. For the smaller pressure ratios (PR=5,10,20) the repeated cell-like structure is comparatively clear in Figs. 7(*a*)–7(*d*), while it is smeared for the case of larger pressure ratio, which may be due to the limit of simulation domain or very lower density level at the far downstream. In addition, one distinct feature in this near-continuum regime (Kn=0.001,0.0005) is the temperature and Mach number scale approximately as $(z/D)^{-5/4}$ [Fig. 7(*b*)] and $(z/D)^{3/4}$ [Fig. 7(*d*)], respectively, before the Mach disk, which is not seen in the transitional regime (Kn=0.1,0.01). Detailed reasons resulting in these special scalings require further study. It may be due to the formation of the shock structure consisting of barrel shock and Mach disk, which prevents the penetration of background gas into the expansion region near the orifice exit. In Fig. 7(*c*), centerline velocity generally increases at first, then decreases rapidly across the Mach disk and finally increase and decrease alternatively further downstream, depending on the pressure ratios. The maximum velocity in this alternative oscillation is generally smaller than the velocity before rapid decrease. It is also found that the maximum rapid decrease of centerline velocity occurs at PR=50 in the current study. Centerline Mach number changes much more pronouncedly due to the change of centerline temperature, which is similar to the case of Kn=0.1 as presented in Fig. 5.

Figure 8 presents the comparison of the Mach-disk position and diameter, respectively, between the simulation in the near-continuum regime (Kn=0.001,0.0005) and the experimental correlation in the continuum limit [8,9,22]. Correlations of Mach-disk position and diameter were determined experimentally as $X_M/D=0.67(P_o/P_b)^{1/2}$ [8] and $D_M/D=0.24(P_o/P_b)^{1/2}$ [9], respectively. Due to the thickened Mach disk in the near-continuum regime, there are uncertainties in determining the accurate position, and especially the diameter, of the Mach disk. Nevertheless, we have defined the position of the Mach disk by locating where the minimum value of the density is. Uncertainty bars are included for the Mach-disk position in the figure for reference, while it is not shown for the Mach-disk diameter due to the difficulty of deciding the uncertainties. Nevertheless, we have measure the radial position at the Mach disk, where the density is maxima, as the Mach-disk position. Results show that the simulated data at Kn=0.001 and 0.0005 in the near-continuum limit are in reasonable agreement with the experimental correlation of Ashkenas and Sherman [8] in the continuum limit, considering the uncertainties as mentioned in the above. Similar agreement can also be found for the Mach-disk diameter as a function of the pressure ratio in Fig. 8.

Figure 9 shows the comparison of the radial profiles of normalized density for Kn=0.1 and Kn=0.001 at different positions (PR=5,000) in the inviscid core, with a simple density cosine-square scaling proposed by Ashkennas and Shermann [8] based on their experimental data. Results show the accuracy of the simple density scaling deteriorates with increasing axial position, although the simple scaling law always predicts a wider radial density profile in general. Reason for the discrepancy requires further

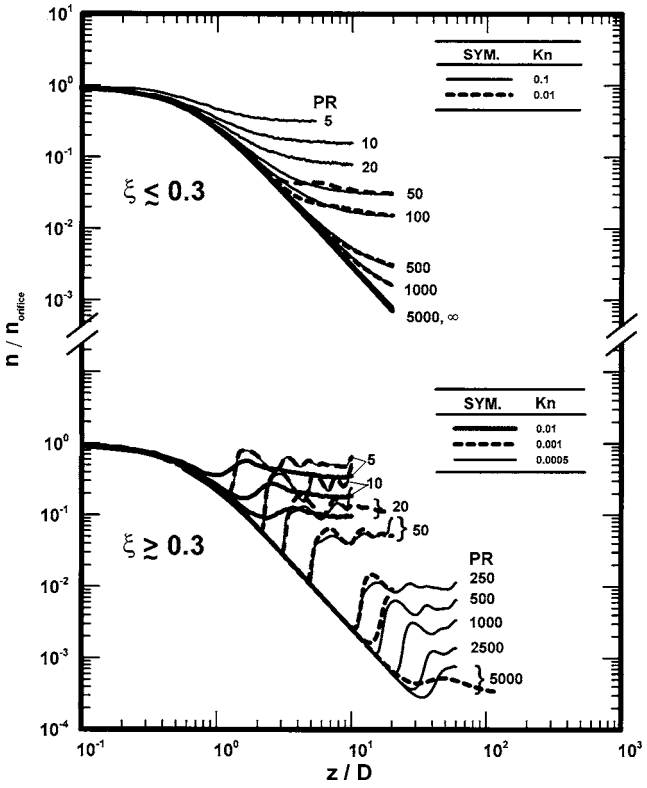

Fig. 10 Flow condition of different ξ

investigation. Flow at Kn=0.001 expands more quickly than that at Kn=0.1 at the same pressure ratio. Similar trends can be found for larger pressure ratios before the Mach disk if it exists.

In Muntz et al. [10], they proposed a rarefaction parameter $\xi = D(p_0 p_b)^{1/2}/T_0$ describing the combined effects of rarefaction and pressure ratio. It is interesting to know the correspondence between this parameter and the cases simulated cases simulated in the current study. Table 1 shows the resulting values for all the simulated cases. Equivalently, previous results can be illustrated using this rarefaction parameter and are shown in Fig. 10. Results clearly show that the cell-like structure (or the Mach disk) begins to appear as $\xi \gtrsim 0.3$ and larger. For $\xi \lesssim 0.3$ the flow can be categorized as the scattering regime as described in [10].

Conclusions

A parallel three-dimensional DSMC method using unstructured solution-based adaptive tetrahedral mesh is used to study flow structure of a single underexpanded argon free jet from transitional to near-continuum regime. In the transitional regime, gas flowing out of the orifice continues to expand to background condition if the pressure ratio is large. Otherwise, it expands first and then compress to the ambient value. In the near-continuum regime, a distinct cell-like flow structure begins to form similar to those obtained in previous experimental study in the continuum regime. Results of simulated Mach-disk position and diameter in the near-continuum regime are in reasonable agreement with previous experimental correlation in the continuum regime. In addition, highly thermal nonequilibrium both occurs across the Mach disk in the near-continuum regime and near the orifice for rapid gas expansion in the transitional regime. One last comment the authors would like to make is the statistical noise near the orifice exits, especially for the cases of Kn=0.0005 and Kn=0.001, which is the near-continuum regime. Thus, the fidelity of the data very near the orifice exit may be in doubt in the current study. From the computational viewpoint, N-S equations should be used in this high-density region instead of the DSMC method, which necessitates the hybrid of the DSMC method and the N-S solver. Preliminary progress toward this goal will be reported elsewhere [23].

Acknowledgments

The authors would like to express their sincere thanks to the computing resources provided by the National Center for High-Speed Computing of National Science Council of Taiwan. In addition, financial support by National Science Council of TAIWAN (NSC91-2212-E-009-045) is also highly appreciated.

References

[1] Phalnikar, K. A., Alvi, F. S., and Shih, C., 2001, "Behavior of Free and Impinging Supersonic Microjets," AIAA Paper No. 2001-3047.
[2] Scroggs, S. D., and Settles, G. S., 1996, "An Experimental Study of Supersonic Microjets," Exp. Fluids, **21**, pp. 401–409.
[3] Adamson, T. C., Jr., 1964, "The Structure of the Rocket Exhaust Plume Without Reaction at Various Altitudes," *Supersonic Flow, Chemical Processes and Radiation Transfer*, Pergamon, New York.
[4] Young, W. S., 1975, "Derivation of the Free-Jet Mach-Disk Location Using the Entropy-Balance Principle," Phys. Fluids, **18**, pp. 1421–1425.
[5] Eastman, D. W., and Radtket, L. P., 1963, "Location of the Normal Shock Wave in the Exhaust Plume of a Jet," AIAA J., **1**, pp. 918–919.
[6] Owen, P. L., and Thornhill, M. A., 1948, "The Flow in an Axially-Symmetric Supersonic Supersonic Jet From a Nearly Sonic Orifice Into a Vacuum," Aeronautical Research Council, ARC Technical Report No. RM-2616.
[7] Love, E. S., Grigsby, C. E., Lee, L. P., and Woodling, M. S., 1959, "Experimental and Theoretical Studies of Axisymmetric Free Jets," NSNA TR R-6.
[8] Ashkenas, H., and Sherman, F. S., 1966, "The Structure and Utilization of Supersonic Free Jets in Low Density Wind Tunnels," *Rarefied Gas Dynamics, Fourth Symposium, Vol. II*, Academic, New York, pp. 84–105.
[9] Crist, S., Sherman, P. M., and Glass, D. R., 1966, "Study of the Highly Under-Expanded Sonic Jet," AIAA J., **4**, pp. 68–71.
[10] Muntz, E. P., Hamel, B. B., and Maguire, B. L., 1970, "Some Characteristics of Exhaust Plume Rarefaction," AIAA J., **8**, pp. 1651–1658.
[11] Bird, G. A., 1994, *Molecular Gas Dynamics and the Direct Simulation of Gas Flows*, Oxford University Press, New York.
[12] Teshima, K., and Usami, M., 1997, "An Experimental Study and DSMC Simulation of Rarefied Supersonic Jets," *20th International Symposium on Rarefied Gas Dynamics*, C. Shen, ed., Bejing University Press, Beijing, pp. 567–572.
[13] Wu, J.-S., Tseng, K.-C., and Wu, F.-Y., 2004, "Parallel Three-Dimensional DSMC Method Using Mesh Refinement and Variable Time-Step Scheme," Comput. Phys. Commun., **162**(3), pp. 166–187.
[14] Wu, J.-S., Tseng, K.-C., and Kuo, C.-H., 2002, "The Direct Simulation Monte Carlo Method Using Unstructured Adaptive Mesh and Its Application," Int. J. Numer. Methods Fluids, **38**(4), pp. 351–375.
[15] Wu, J.-S., and Tseng, K.-C., 2003, "Concurrent DSMC Method Using Dynamic Domain Decomposition," *23rd International Symposium on Rarefied Gas Dynamics*, A. Ketsdever and E. Muntz, eds., AIP Conf. Proc. **663**, pp. 406–413.
[16] Wu, J.-S. and Tseng, K.-C., 2005, "Parallel DSMC Method Using Dynamic Domain Decomposition," Int. J. Numer. Methods Eng., **63**, pp. 37–76.
[17] Kannenberg, K. C., 1998, "Computational Method for the Direct Simulation Monte Carlo Technique With Application to Plume Impingement," Ph.D. thesis, Cornell University, Ithaca.
[18] Wu, J.-S., and Lian, Y.-Y., 2003, "Parallel Three-Dimensional Direct Simulation Monte Carlo Method and Its Applications," Comput. Fluids, **32**(8), pp. 1133–1160.
[19] Wu, J.-S., Lee, Fred, and Wong, S.-C., 2001, "Pressure Boundary Treatment In Micromechanical Devices Using The Direct Simulation Monte Carlo Method," JSME Int. J., Ser. B, **44**(3), pp. 439–450.
[20] Walshaw, C., Cross, M., and Everett, M., 1997, "Parallel Dynamic Graph Partitioning for Adaptive Unstructured Meshes," J. Parallel Distrib. Comput., **47**, pp. 102–108.
[21] Nicol, D. M., and Saltz, J. H., 1988, "Dynamic Remapping of Parallel Computations With Varying Resource Demands," IEEE Trans. Comput., **39**(9), pp. 1073–1087.
[22] Mirels, H., and Mullen, J. F., 1963, "Expansion of Gas Clouds and Hypersonic Jets Bounded by a Vacuum," AIAA J., **1**, pp. 596–602.
[23] Wu, J.-S., Lian, Y.-Y., Gary Cheng, and Roy Koomullil, 2005, "Development of a Parallel Hybrid Method for the DSMC and NS Solver," AIAA 43rd Aerospace Sciences Meeting and Exhibit, Reno Hilton, Jan, pp. 10–13.